Spin injection and transport in a solution-processed organic semiconductor at room temperature

S. Mooser,[1] J. F. K. Cooper,[1] K. K. Banger,[1] J. Wunderlich,[2,3] and H. Sirringhaus[1,*]

[1]*Cavendish Laboratory, University of Cambridge, Cambridge CB3 0HE, United Kingdom*
[2]*Hitachi Cambridge Laboratory, Cambridge CB3 0HE, United Kingdom*
[3]*Institute of Physics ASCR, v.v.i., Cukrovarnickà 10, 162 53 Praha 6, Czech Republic*

Spin injection and transport in solution-processed 6,13-*bis*(triisopropylsilylethynyl)-pentacene (TIPS-pentacene) are investigated using vertical CoPt/TIPS-pentacene/AlOx/Co spin valve architectures. The morphology and the molecular orientation of TIPS-pentacene spin-coated from a chloroform solution as grown in the spin valve devices are characterized by means of atomic force microscopy and x-ray diffraction, where the π-π stacking is found to be in planes oriented parallel to the substrate plane on CoPt (not $L1_0$-ordered). The magnetization hysteresis loops recorded with a superconducting quantum interference device show an individual switching of the magnetization of the two ferromagnetic layers. The antiparallel state of the relative orientation of CoPt and Co is achieved due to their different coercive fields. A spin valve effect is observed at room temperature. The scaling of the magnetoresistance (MR) with the bulk mobility of TIPS-pentacene as a function of temperature together with the dependence of the MR on the interlayer thickness clearly indicates spin injection and transport in TIPS-pentacene. From organic semiconductor-spacer thickness-dependent MR measurements, we estimate a spin relaxation length of TIPS-pentacene of $\lambda_s = (24 \pm 6)$ nm and a spin relaxation time of approximately $\tau_s = 3.5$ μs at $T = 300$ K, taking the measured bulk mobility of holes into account.

I. INTRODUCTION

Recently, growing interest in the field of organic semiconductors (OSCs) has extended from the complex aspects of charge carrier transport to the study of the spin degree of freedom and its propagation in those anisotropic and partly localized systems.[1] The first experimental detection of spin injection into an OSC was published in 2002,[2] where two ferromagnetic (FM) La$_{0.7}$Sr$_{0.3}$MnO$_3$ (LSMO) electrodes were separated by a 70–500 nm long channel of sexithiophene (T6) in a lateral spin device. A magnetoresistance (MR) was measured up to room temperature in devices with a channel length of up to 200 nm. Even though this work demonstrated organic materials to be attractive for long-distance spin transport, a relationship between the MR and the relative orientation of the magnetization of the LSMO contacts could not be elucidated. In 2004, Xiong *et al.*[3] prepared vertical spin valves based on a tris(8-hydroxyquinoline)aluminum(III) (Alq$_3$) film sandwiched between LSMO and Co. This device exploits the different coercivities of LSMO and Co, where a MR of approximately 40% at $T = 11$ K for a spacer thickness of 130 nm was observed. After these discoveries, a series of spin valves with different combinations of FM electrodes and OSCs as interlayers were investigated (e.g., Refs. 4–11). However, there is an ongoing debate as to whether the MR signals observed in organic spin valves are due to a tunneling magnetoresistance (TMR), a multistep tunneling MR, or a giant magnetoresistance (GMR) effect,[12–14] and what the contributions of interface effects such as the tunneling anisotropic magnetoresistance (TAMR) in organic spin valves[15] are. Here, we study spin transport in thin films of the solution-processed small molecule 6,13-*bis*(triisopropylsilylethynyl)-pentacene (TIPS-pentacene), a *p*-type OSC which has recently attracted particular interest in organic thin-film transistors as it exhibits a negative temperature coefficient of the in-plane mobility due to localized transport limited by thermal lattice fluctuations.[16]

In vertical spin valves with the OSC sandwiched between two FM metal contacts, we observe clear evidence for spin transport in the bulk of the OSC. The MR signal scales with the bulk mobility of TIPS-pentacene as a function of temperature and with the thickness of the OSC layer. In order to enable such investigations of the bulk spin transport, we work deliberately with relatively thick OSC films. This inevitably leads to relatively small MR values compared to previously reported GMR and TMR structures with OSC thicknesses in the tunneling regime[17,18] that naturally exhibit higher MR values. However, such tunnel junctions do not allow direct investigation of the bulk spin transport properties of the OSC itself. We emphasize that in this work our aim is not to achieve high MR values, but to investigate the correlation between the spin diffusion length and charge carrier mobility in the bulk of TIPS-pentacene. Furthermore, we focus on a temperature range between room temperature and about $T = 150$ K, where the charge carrier mobility remains relatively high. In contrast, the high MR values in GMR and TMR structures were only observed at low temperatures below $T = 80$–100 K.

II. DEVICE FABRICATION AND MEASUREMENTS

In order to investigate spin transport in solution-processed TIPS-pentacene, vertical spin valve architectures with the following structure from bottom to top were prepared: Si/SiO$_2$/Pt/CoPt/TIPS-pentacene/AlOx/Co/Al (Fig. 1).

The devices were fabricated on Si wafers with 300 nm of thermally grown SiO$_2$ which were cleaned with DI water, isopropanol, and acetone, in an ultrasonic bath followed by oxygen plasma ashing. The bottom electrodes were patterned by standard photolithography and a double-layer lift-off process. Pt and CoPt were deposited at room temperature by dc sputtering in a CEVP magnetron sputtering system with a base pressure of 10^{-8} mbar, where the growth pressure amounted to
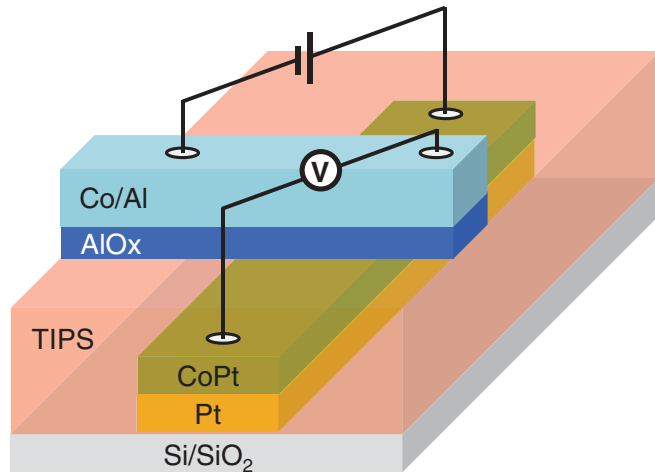
III. EXPERIMENTAL RESULTS AND DISCUSSION

A. Morphology and crystal orientation

TIPS-pentacene was spin-coated from an anhydrous chloroform solution. Chloroform exhibits a low boiling point of 61.2 °C which results in smooth TIPS-pentacene films with a root mean squared (rms) roughness of 0.35 nm on a 1 μm^2 area as shown by AFM [Fig. 2(a)]. Higher boiling point solvents such as toluene and 1,2,3,4-tetrahydronaphthalene (tetralin)
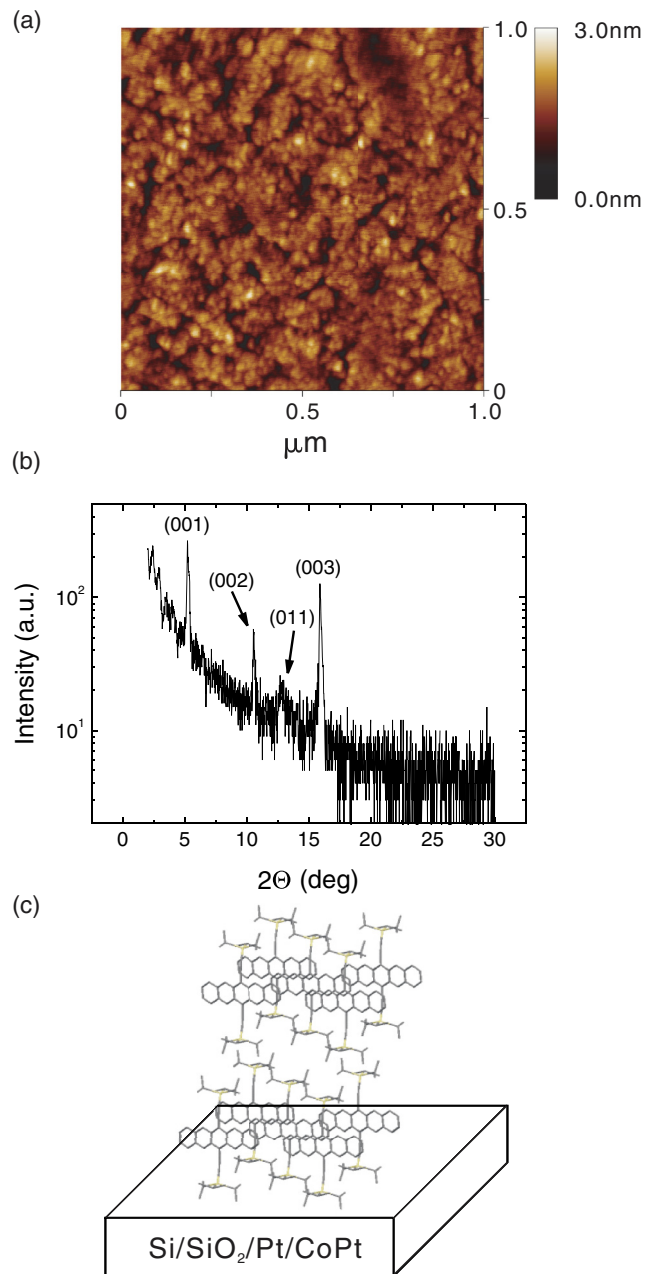

(a)

(b)

(c)

FIG. 2. (Color online) (a) AFM image of a TIPS-pentacene film spin-coated from a 15 g/l anhydrous chloroform solution on Si/SiO$_2$ (300 nm)/Pt (5 nm)/CoPt (10 nm). (b) Low-angle x-ray diffraction scan of a 150 nm thin TIPS-pentacene film spin-coated from a 25 g/l chloroform solution on the identical substrate as in (a). (c) Schematic of the molecular orientation of TIPS-pentacene on Si/SiO$_2$ (300 nm)/Pt (5 nm)/CoPt (10 nm).

FIG. 1. (Color online) Schematic of a typical spin valve device. The two ferromagnetic layers CoPt and Co are separated by the organic semiconductor TIPS-pentacene and a thin AlOx tunnel barrier. Pt and Al serve as adhesive buffer layer and capping layer, respectively.

2×10^{-3} mbar. The Pt buffer layer (5 nm) was grown at a rate of 0.06 Å/s, the CoPt films (10 nm) were co-sputtered at a rate of 0.18 Å/s and had a final monolayer equivalent growth of Pt on top to minimize any possible oxidation. TIPS-pentacene was then spin-coated from an anhydrous chloroform solution with varying concentration (15–25 g/l depending on the thickness required) and spinning parameters in a nitrogen glove box in order to perform thickness-dependent magnetic transport measurements. A 2 nm aluminum oxide (AlOx) layer was deposited on top of TIPS-pentacene by thermal evaporation of Al through a shadow mask with a rate of approximately 3–4 Å/s and a base pressure of 10^{-6} mbar, and subsequent oxidation in air for several hours. It has been shown that introducing an AlOx tunnel barrier between the OSC and the FM counterelectrode avoids the formation of an ill-defined layer due to penetration of the counterelectrode into the OSC.[5] In addition, no chemical reactions occur at the interface.[19] Furthermore, a fast deposition rate was used to avoid penetration of the metal into the OSC.[20–22] A 10 nm thin Co film was then deposited by e-beam evaporation through a shadow mask at a base pressure of 10^{-6} mbar with a rate of 0.2–0.3 Å/s and subsequently capped with 5 nm of thermally evaporated Al with a rate of 1.5–2 Å/s before taking the samples out of the vacuum chamber. The overlap area of the crossbar configuration of the spin valve amounted to 1 mm^2.

The morphology of TIPS-pentacene was characterized with a Veeco Digital Instruments Dimension 3100 AFM. X-ray diffraction (XRD) measurements were obtained with a Philips PW1820 diffractometer in a Bragg-Brentano geometry. The magnetic properties of the films were measured in a Quantum Design SQUID magnetometer. Four-point probe electrical and magnetic field-dependent transport measurements were performed using a Keithley 236 source measure unit together with an HP 34401A multimeter, where the sample was placed in a ^{4}He bath cryostat containing a superconducting magnet.

evaporate at a slower rate during spin-coating, enabling the films to form highly crystalline structures which increases the in-plane charge carrier mobility in organic field-effect transistors (FETs).[16,23] However, large crystals also increase the surface roughness and potentially lead to pinholes in vertical devices. Hence, chloroform was the preferred solvent in this study and it allowed for thickness-dependent transport measurements of the spin valves. Figure 2(b) shows a low-angle XRD scan of a TIPS-pentacene film spin-coated on Si/SiO$_2$/Pt/CoPt to mimic its growth as in the actual spin valve devices. It can be seen that the film is polycrystalline with the π-π stacking in planes parallel to the substrate plane on CoPt [see schematic in Fig. 2(c)]. The layer-by-layer separation was calculated to be 16.9 Å. It is to be noted that the (011) peak in the XRD scan is a result of some grains of TIPS-pentacene having a component of the π-π stacking direction out-of-plane. These grains could have a major contribution to the electrical transport in the MR measurements.

B. Magnetic properties of the spin valves

CoPt served as the bottom FM electrode. It exhibits a high magnetic anisotropy due to a large spin-orbit coupling strength introduced by the Pt atoms. This leads to a higher coercive field of CoPt compared to Co, allowing for an antiparallel state of the magnetization of the two FM layers, which is a prerequisite for the successful operation of a spin valve. CoPt is a magnetic alloy where the disordered phase shows a face-centered cubic (fcc) crystalline structure with the Co and Pt atoms occupying random sites of the lattice. Upon annealing at high temperatures of around 650 °C, a phase transition from the disordered fcc to an ordered face-centered tetragonal (fct)—also called $L1_0$—crystal can be observed,[24,25] where the tetragonal distortion is caused by the 3d and 5d atomic size mismatch between Co and Pt so that the cubic symmetry is broken [$c/a = 0.975$ (Ref. 26)]. However, $L1_0$-ordered CoPt exhibits an easy axis of magnetization out-of-plane. Since

an in-plane easy axis is required for the operation of the spin valves when using in-plane magnetized Co as a counter electrode, the Co content of the CoPt layer in this study was increased (ratio Co : Pt = 1 : 0.9 based on their respective molar volumes). The film was deposited at room temperature and no postannealing was performed. The disordered phase of the CoPt films was confirmed by XRD, where no diffraction peaks were observed (not shown). Besides its high anisotropy, CoPt has been considered an interesting material for room temperature spintronics devices because of its high Curie temperature of approximately $T = 750$ K due to a large exchange splitting of the Co atoms.[27] This property of CoPt is a potential advantage over LSMO, which is often used in organic spin valves due to its half-metallicity at low temperatures; however, the Curie temperature of LSMO of approximately $T = 340$ K could inhibit room temperature applications.

The magnetization hysteresis loops of the spin valves were recorded in a SQUID magnetometer and are presented in Fig. 3. Additionally, in order to illustrate the magnetic properties

FIG. 4. (Color online) (a) Magnetoresistance (MR) loop of a Pt (5 nm)/CoPt (10 nm)/TIPS-pentacene (75 nm)/AlOx (2 nm)/Co (10 nm)/Al (5 nm) spin valve measured at $T = 300$ K and $V_b = 1$ V. The blue (▲) and red (○) curves denote the MR response for increasing and decreasing magnetic fields, respectively. The insets show the relative orientation of the ferromagnetic electrodes for parallel (P) and antiparallel (AP) states, respectively. (b) Bias voltage dependence of the MR value for the device in (a) measured at $T = 300$ K. Positive bias refers to hole injection into TIPS-pentacene via the CoPt layer.
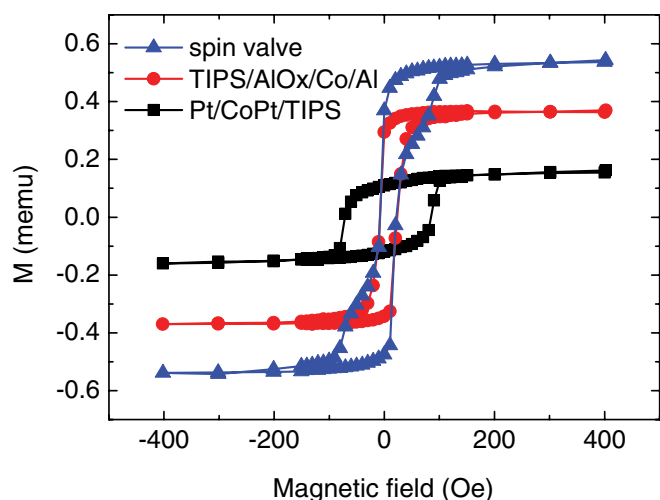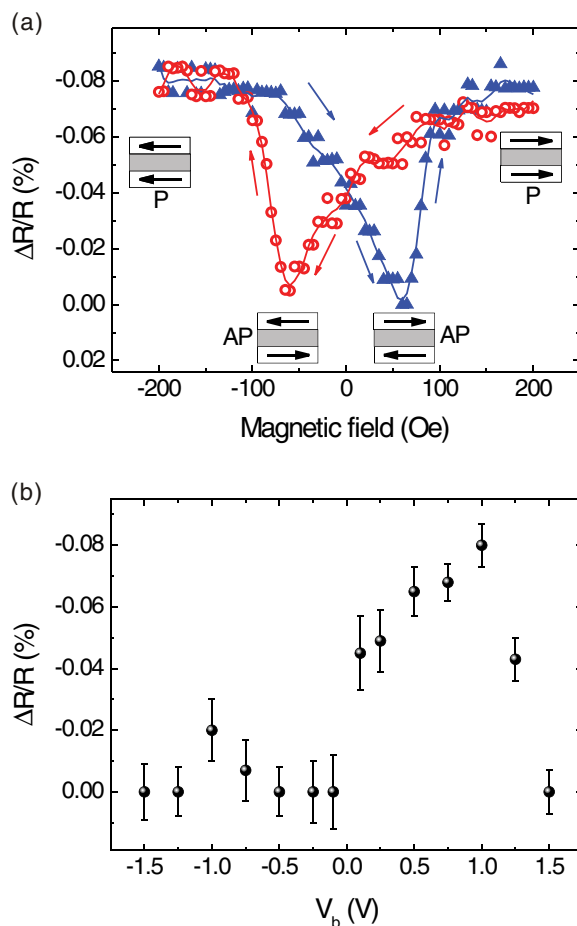

FIG. 3. (Color online) Magnetization hysteresis loops of (▲) a spin valve with 35 nm TIPS-pentacene, as well as (●) a 10 nm thin Co film and (■) a 10 nm CoPt film deposited under the same conditions as the respective ferromagnetic electrodes in the actual spin valve devices with 35 nm TIPS-pentacene, measured at $T = 300$ K.

of the two FM layers individually as prepared in the spin valve devices, the magnetization hysteresis curves of TIPS-pentacene (35 nm)/AlOx (2 nm)/Co (10 nm)/Al (5 nm) and Pt (5 nm)/CoPt (10 nm)/TIPS-pentacene (35 nm) deposited on a Si/SiO$_2$ (300 nm) wafer, respectively, are displayed. A clear individual switching of the two FM layers separated by TIPS-pentacene was observed which enables an antiparallel state of the spin valves upon applying an external magnetic field, where the different coercive fields of Co ($H_c = 15$ Oe at $T = 300$ K) and CoPt ($H_c = 80$ Oe at $T = 300$ K) are exploited. Note that the lateral dimensions of the samples varied, such that the magnitude of the saturation magnetization cannot be compared.

C. Room temperature magnetoresistance

MR measurements were performed in a cryostat containing a superconducting magnet. The result of a Si/SiO$_2$ (300 nm)/Pt (5 nm)/CoPt (10 nm)/TIPS-pentacene (75 nm)/AlOx (2 nm)/Co (10 nm)/Al (5 nm) spin valve measured at $T =$ 300 K and a bias voltage of $V_b = 1$ V (positive bias refers to hole injection into TIPS-pentacene via the CoPt layer) is shown in Fig. 4(a). A spin valve effect of 0.08% in magnitude was obtained, where the change in resistance corresponds well with the relative orientation of the magnetization of the two

FM layers as observed in the hysteresis loops. The origin of the spin valve effect where the resistance of the device is lower for the antiparallel state has recently been discussed by Barraud *et al.*[18] It is suggested that when the FM metal and the OSC are in contact, new hybrid electronic states can occur at the interface which act as an additional spin filter. As a result, the spin polarization of the injected current can be different and even opposite in sign. Figure 4(b) displays the bias voltage dependence of the MR value for the spin valve shown in Fig. 4(a). The negative MR was found to be asymmetric with respect to the bias voltage polarity. For positive V_b, i.e., hole injection into TIPS-pentacene via the CoPt electrode, the MR is larger compared to negative V_b, where the spin-polarized holes were injected from the Co counterelectrode through the AlOx tunnel barrier. Since the current is almost symmetric with respect to the bias voltage polarity in the spin valves [as shown later in Fig. 5(c)], the asymmetry in the V_b dependence of the MR originates from a better spin injection efficiency via the CoPt bottom electrode compared to the AlOx/Co counterelectrode. Furthermore, the MR varies with the magnitude of the applied V_b, where it increases with increasing V_b up to $|V_b| = 1$ V and vanishes above $|V_b| = 1.5$ V. The decrease of the MR for large $|V_b|$ has been explained by an increase of the charge carrier–magnon scattering in the FM contacts upon current increase.[28,29] Moreover, for charge carrier–magnon
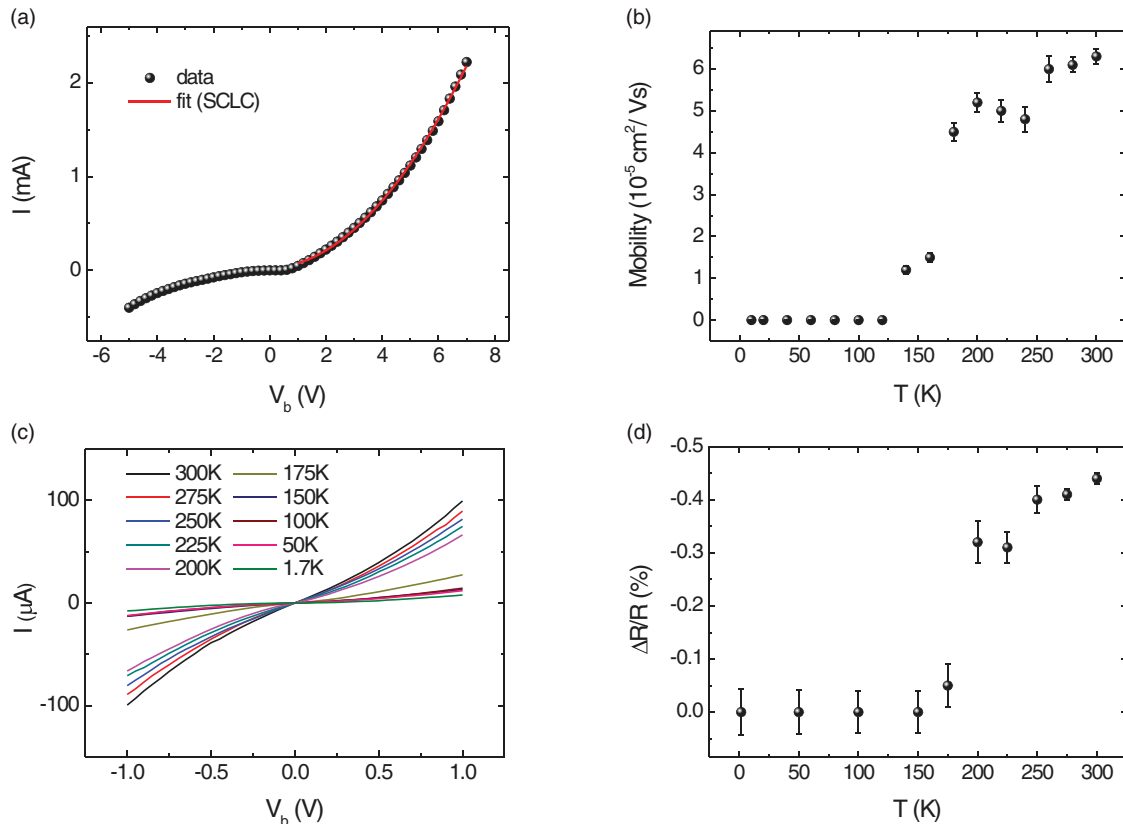

FIG. 5. (Color online) (a) *I(V)* characteristics of a Si/SiO$_2$ (300 nm)/Pt (5 nm)/CoPt (10 nm)/TIPS-pentacene (180 nm)/MoO$_3$ (10 nm)/Au (40 nm) device measured at $T = 300$ K. Positive bias refers to hole injection into TIPS-pentacene from the MoO$_3$/Au electrode. The red curve shows the fit to the space-charge-limited current (SCLC, Mott-Gurney equation: $I \propto V^2$). (b) Bulk mobility of holes in TIPS-pentacene as a function of temperature extracted from the space-charge-limited regime of the device displayed in (a). (c) *I(V)* characteristics of a spin valve device with 40 nm thin TIPS-pentacene for different temperatures. (d) Magnetoresistance as a function of temperature for the device in (c) measured at $V_b = 1$ V.

interactions, the MR dependence on V_b is expected to be asymmetric in asymmetric devices,[30,31] as observed in our spin valves.

D. Temperature-dependent transport and magnetoresistance measurements

A scaling of the MR with respect to the bulk mobility of the charge carriers in the semiconducting interlayer is strong evidence for successful spin injection and transport in the OSC, as opposed to a tunneling or multitunneling process. In order to obtain a temperature-dependent value for the bulk mobility of the charge carriers in TIPS-pentacene along the direction of the side chains, a vertical diode of Si/SiO$_2$ (300 nm)/Pt (5 nm)/CoPt (10 nm)/TIPS-pentacene (180 nm)/MoO$_3$ (10 nm)/Au (40 nm) was prepared in a crossbar configuration with an overlap area of 1 mm^2, where the $I(V)$ characteristics were recorded at different temperatures from $T = 300$ K down to $T = 10$ K. The MoO$_3$ and Au films were prepared by thermal evaporation at a base pressure of 10^{-6} mbar and a deposition rate of 0.3 Å/s and 1.0 Å/s, respectively. The Pt/CoPt bottom contact was used to guarantee the same growth of TIPS-pentacene during spin-coating as in the spin valve devices. Furthermore, an Ohmic contact between MoO$_3$/Au and TIPS-pentacene allows for extracting the mobility of holes in TIPS-pentacene from the space-charge-limited regime using the Mott-Gurney equation, where $I \propto V^2$ (Ref. 32). The $I(V)$ characteristics measured at $T = 300$ K and the respective fit to the Mott-Gurney equation are shown in Fig. 5(a). The room temperature mobility amounts to $\mu = 6.3 \times 10^{-5}$ cm^2/V s. This low value is a clear indication of hopping transport along the direction of the side chains, as opposed to a bandlike transport behavior along the π-π stacking direction observed for TIPS-pentacene in a gated FET,[16] where the mobility reaches room temperature values of up to $\mu = 1$ cm^2/V s. Figure 5(b) displays the bulk mobility of holes in TIPS-pentacene as a function of temperature extracted from the space-charge-limited regime. A drop in the mobility from $\mu = 4.5 \times 10^{-5}$ cm^2/V s at $T = 180$ K to $\mu = 1.5 \times 10^{-5}$ cm^2/V s at $T = 160$ K was observed. At temperatures below $T = 120$ K, the mobility drops to $\mu = 10^{-9} - 10^{-8}$ cm^2/V s, and the current is negligibly small. This result is in accordance with the behavior of the field-effect mobility of holes in an FET, where a decrease for temperatures below $T = 150$ K can be found.[16] The drop in mobility in the range from $T = 180$ K to $T = 160$ K manifests itself as well in the drop of the current in the actual spin valve device as shown in Fig. 5(c), where the $I(V)$ characteristics of a spin valve with a TIPS-pentacene thickness of 40 nm are displayed for temperatures ranging from $T = 300$ K down to $T = 1.7$ K. Finally, a similar behavior of the MR as a function of temperature was observed in the spin valves, as shown here for a device with a TIPS-pentacene thickness of 40 nm measured at $V_b = 1$ V [Fig. 5(d)]. The MR drops from 0.32% at $T = 200$ K to 0.05% at $T = 175$ K and becomes too low to measure for temperatures below $T = 175$ K as a result of a small spin relaxation length due to a low mobility of the charge carriers. This effect overcomes an increase of the spin relaxation time for lower temperatures,[33] such that no MR was observed within the measurement sensitivity. The

magnitude of the MR depends on the spin relaxation length (λ_s) [see Eq. (1)], which in turn is given by $\lambda_s = \sqrt{D \tau_s}$ (Ref. 33), where D is the spin diffusion coefficient and τ_s is the spin relaxation time. Since D is related to the mobility via the Einstein relation, the scaling of the MR with the bulk mobility of TIPS-pentacene is conclusive evidence for spin injection and transport in TIPS-pentacene. Moreover, this distinct temperature dependence of the MR allows us to exclude that the magnetic field dependence of the resistance is caused instead by the anisotropic magnetoresistance (AMR) or TAMR effect. This result is strongly supported by the dependence of the MR on the OSC thickness. In order to estimate the spin relaxation length of TIPS-pentacene in the direction of the side chains, the MR was measured as a function of the TIPS-pentacene thickness, which was varied between 40 nm and 100 nm (the MR becomes too low to measure for a TIPS-pentacene thickness of 120 nm). The result is shown in Fig. 6(a). The right axis in Fig. 6(a) displays the absolute change of resistance of the spin valves when being switched from the parallel to the antiparallel magnetization configuration. As a reference, the resistance value of the spin valves measured at $T = 300$ K and $V_b = 1$ V is presented in
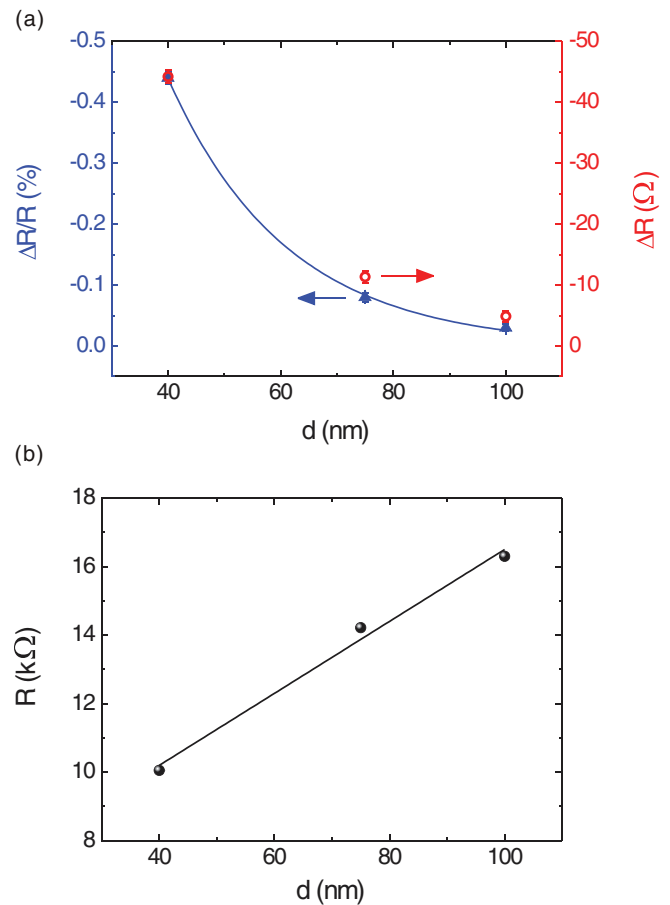

FIG. 6. (Color online) (a) (▲, left axis) Magnetoresistance and (○, right axis) absolute change of the resistance of the spin valves as a function of the TIPS-pentacene thickness, measured at $T = 300$ K and $V_b = 1$ V. (b) Resistance of the spin valves as a function of the TIPS-pentacene thickness at $T = 300$ K and $V_b = 1$ V.

Fig. 6(b). Applying a modified Jullière formula,[34] in which the decay of the spin polarization of the injected carriers in the OSC is taken into account, so that the MR is given by[3]

$$\text{MR} = \frac{2p_1 p_2 e^{-d/\lambda_s}}{1 - p_1 p_2 e^{-d/\lambda_s}}, \tag{1}$$

where p_1 and p_2 denote the spin polarization of CoPt and Co, respectively, assuming no loss of spin at the interface, and d is the OSC thickness, results in the fit in Fig. 6(a), where the following parameters can be obtained (the ill-defined layer due to metal penetration into the OSC during deposition of the counterelectrode on top of TIPS-pentacene is assumed to be zero due to the AlOx interlayer[5]): $\lambda_s = 24$ nm, $p_1 p_2 = 0.014$. The reduction of $p_1 p_2$ compared to literature values[35] is presumably due to a poor spin injection efficiency from the FM metal into TIPS-pentacene, which is not accounted for in Eq. (1). Furthermore, the low effective spin polarization of CoPt and Co, respectively, together with a large TIPS-pentacene thickness, results in comparatively low MR values due to bulk spin transport, as opposed to organic magnetic tunnel junctions, where MR values of more than 300% have been achieved for interlayer thicknesses of the OSC of less than 2 nm.[18] Our choice of such thick films here is deliberate in order to establish the relationship between the MR effect and spin transport in the bulk of the OSC.

It is to be noted that a spin relaxation length ranging from 18 nm up to 30 nm can be obtained from accurate fits to the data. The room temperature spin relaxation length of $\lambda_s = 24$ nm together with a bulk mobility of $\mu = 6.3 \times 10^{-5}$ cm^2/V s in a diode structure yields a spin relaxation time of approximately $\tau_s = 3.5$ μs. This result is in accordance with values obtained for other OSCs, where a low spin-orbit coupling together with small carrier mobilities leads to long spin lifetimes and short spin relaxation lengths.[36]

IV. CONCLUSION

In summary, we have studied spin transport in thin films of the solution-processed small molecule TIPS-pentacene as a function of OSC thickness using vertical CoPt/TIPS-pentacene/AlOx/Co spin valve architectures. We report on the scaling of the MR response with respect to the bulk mobility of the charge carriers in an OSC as a function of temperature, which is strong evidence for spin transport in TIPS-pentacene. It will be interesting to investigate whether this behavior is universal and can also be observed in other OSCs, such as Alq$_3$. Our results suggest that a careful selection of materials might open the door to organic spintronics performed at room temperature, where the OSC serves as the spin-transporting material.

*hs220@cam.ac.uk

[1] V. Dediu, L. Hueso, I. Bergenti, and C. Taliani, Nat. Mater. **8**, 707 (2009).

[2] V. Dediu, M. Murgia, F. C. Matacotta, C. Taliani, and S. Barbanera, Solid State Commun. **122**, 181 (2002).

[3] Z. Xiong, D. Wu, Z. Vardeny, and J. Shi, Nature (London) **427**, 821 (2004).

[4] F. J. Wang, C. G. Yang, Z. V. Vardeny, and X. G. Li, Phys. Rev. B **75**, 245324 (2007).

[5] V. Dediu, L. E. Hueso, I. Bergenti, A. Riminucci, F. Borgatti, P. Graziosi, C. Newby, F. Casoli, M. P. De Jong, C. Taliani, and Y. Zhan, Phys. Rev. B **78**, 115203 (2008).

[6] S. Majumdar, H. S. Majumdar, R. Laiho, and R. Österbacka, J. Alloys Compd. **423**, 169 (2006).

[7] W. Xu, G. J. Szulczewski, P. LeClair, I. Navarrete, R. Schad, G. Miao, H. Guo, and A. Gupta, Appl. Phys. Lett. **90**, 072506 (2007).

[8] N. A. Morley, A. Rao, D. Dhandapani, M. R. J. Gibbs, M. Grell, and T. Richardson, J. Appl. Phys. **103**, 07F306 (2008).

[9] F. Wang, Z. Xiong, D. Wu, J. Shi, and Z. Vardeny, Synth. Met. **155**, 172 (2005).

[10] T. Shimada, H. Nogawa, T. Noguchi, Y. Furubayashi, Y. Yamamoto, Y. Hirose, T. Hitosugi, and T. Hasegawa, Jpn. J. Appl. Phys. **47**, 1184 (2008).

[11] S. Majumdar, R. Laiho, P. Laukkanen, I. J. Vayrynen, H. S. Majumdar, and R. Österbacka, Appl. Phys. Lett. **89**, 122114 (2006).

[12] R. Lin, F. Wang, J. Rybicki, M. Wohlgenannt, and K. A. Hutchinson, Phys. Rev. B **81**, 195214 (2010).

[13] J.-W. Yoo, H. W. Jang, V. N. Prigodin, C. Kao, C. B. Eom, and A. J. Epstein, Phys. Rev. B **80**, 205207 (2009).

[14] J. J. H. M. Schoonus, P. G. E. Lumens, W. Wagemans, J. T. Kohlhepp, P. A. Bobbert, H. J. M. Swagten, and B. Koopmans, Phys. Rev. Lett. **103**, 146601 (2009).

[15] M. Grünewald, M. Wahler, F. Schumann, M. Michelfeit, C. Gould, R. Schmidt, F. Würthner, G. Schmidt, and L. W. Molenkamp, Phys. Rev. B **84**, 125208 (2011).

[16] T. Sakanoue and H. Sirringhaus, Nat. Mater. **9**, 736 (2010).

[17] J. H. Shim, K. V. Raman, Y. J. Park, T. S. Santos, G. X. Miao, B. Satpati, and J. S. Moodera, Phys. Rev. Lett. **100**, 226603 (2008).

[18] C. Barraud, P. Seneor, R. Mattana, S. Fusil, K. Bouzehouane, C. Deranlot, P. Graziosi, L. Hueso, I. Bergenti, V. Dediu, F. Petroff, and A. Fert, Nat. Phys. **6**, 615 (2010).

[19] M. Popinciuc, H. T. Jonkman, and B. J. van Wees, J. Appl. Phys. **101**, 093701 (2007).

[20] J. H. Cho, D. H. Kim, Y. Jang, W. H. Lee, K. Ihm, J.-H. Han, S. Chung, and K. Cho, Appl. Phys. Lett. **89**, 132101 (2006).

[21] J. Kwon, Y. G. Seol, N.-E. Lee, and I. Chung, J. Vac. Sci. Technol. A **28**, 879 (2010).

[22] A. Dürr, F. Schreiber, M. Kelsch, H. Carstanjen, and H. Dosch, Adv. Mater. **14**, 961 (2002).

[23] J.-F. Chang, B. Sun, D. W. Breiby, M. M. Nielsen, T. I. Sölling, M. Giles, I. McCulloch, and H. Sirringhaus, Chem. Mater. **16**, 4772 (2004).

[24] H. Zeng, M. L. Yan, N. Powers, and D. J. Sellmyer, Appl. Phys. Lett. **80**, 2350 (2002).

[25] K. Yamaguchi, Z. Zhao, C. Chen, M. Hashimoto, J. Shi, and Y. Nakamura, Thin Solid Films **459**, 165 (2004).

[26] A. B. Shick and O. N. Mryasov, Phys. Rev. B **67**, 172407 (2003).

[27] A. B. Shick, F. Máca, J. Mašek, and T. Jungwirth, Phys. Rev. B **73**, 024418 (2006).

[28] A. M. Bratkovsky, Phys. Rev. B **56**, 2344 (1997).

[29] S. Zhang, P. M. Levy, A. C. Marley, and S. S. P. Parkin, Phys. Rev. Lett. **79**, 3744 (1997).

[30] M. Bowen, A. Barthélémy, M. Bibes, E. Jacquet, J.-P. Contour, A. Fert, F. Ciccacci, L. Duò, and R. Bertacco, Phys. Rev. Lett. **95**, 137203 (2005).

[31] R. Y. Gu, L. Sheng, and C. S. Ting, Phys. Rev. B **63**, 220406 (2001).

[32] M. Lampert and P. Mark, *Current Injection in Solids* (Academic, New York, 1970) .

[33] I. Žutić, J. Fabian, and S. Das Sarma, Rev. Mod. Phys. **76**, 323 (2004).

[34] M. Jullière, Phys. Lett. A **54**, 225 (1975).

[35] R. J. Soulen Jr., J. M. Byers, M. S. Osofsky, B. Nadgorny, T. Ambrose, S. F. Cheng, P. R. Broussard, C. T. Tanaka, J. Nowak, J. S. Moodera, A. Barry, and J. M. D. Coey, Science **282**, 85 (1998).

[36] G. Szulczewski, S. Sanvito, and M. Coey, Nat. Mater. **8**, 693 (2009).